Spectral contamination between diffraction orders of the NIR spectrometer (TGO) but possible solutions to overcome it

Abdanour Irbah, Jean-Loup Bertaux, Franck Montmessin, Léa Scheveiler, Gaetan Lacombe, Nicolas Rouanet, Alexander Trokhimovskiy, Oleg Korablev, Anna Fedorova

Spectral contamination between diffraction orders of the NIR spectrometer (TGO) but possible solutions to overcome it

Abdanour Irbah, Jean-Loup Bertaux, Franck Montmessin, Léa Scheveiler, Gaetan Lacombe, et al.

Abdanour Irbah, Jean-Loup Bertaux, Franck Montmessin, Léa Scheveiler, Gaetan Lacombe, Nicolas Rouanet, Alexander Trokhimovskiy, Oleg Korablev, Anna Fedorova, "Spectral contamination between diffraction orders of the NIR spectrometer (TGO) but possible solutions to overcome it ," Proc. SPIE 12777, International Conference on Space Optics — ICSO 2022, 127776Z (12 July 2023); doi: 10.1117/12.2691362

SPIE.

Event: International Conference on Space Optics — ICSO 2022, 2022, Dubrovnik, Croatia

International Conference on Space Optics—ICSO 2022

Dubrovnik, Croatia

3–7 October 2022

Edited by Kyriaki Minoglou, Nikos Karafolas, and Bruno Cugny,

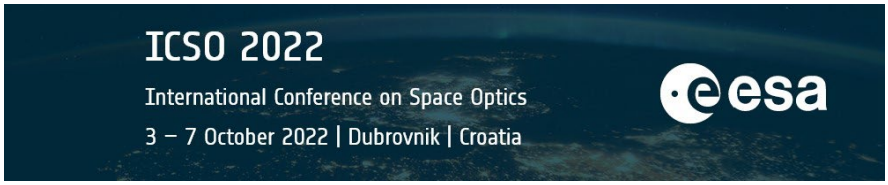

Spectral contamination between diffraction orders of the NIR spectrometer (TGO) but possible solutions to overcome it

International Conference on Space Optics — ICSO 2022, edited by Kyriaki Minoglou, Nikos Karafolas, Bruno Cugny, Proc. of SPIE Vol. 12777, 127776Z · © 2023 ESA and CNES · 0277-786X · doi: 10.1117/12.2691362

Spectral contamination between diffraction orders of the NIR spectrometer (TGO) but possible solutions to overcome it

Abdanour Irbah[a], Jean-Loup Bertaux[a], Franck Montmessin[a], Scheveiler Léa[a], Gaetan Lacombe[a], Nicolas Rouanet[a], Alexander Trokhimovskiy[b], Oleg Korablev[b], and Anna Fedorova[b]

[a]LATMOS/IPSL, UVSQ Université Paris-Saclay, Sorbonne Université, CNRS, 11 BD D'Alembert, 78280 Guyancourt, France
[b]Space Research Institute (IKI), 84/32 Profsoyuznaya, 117997 Moscow, Russia

ABSTRACT

The ACS-NIR spectrometer aboard TGO is currently used to probe the atmosphere of Mars. ACS-NIR detects the spectral signature of atmospheric components along its line of sight as it passes through the atmosphere when the spectrometer points toward the Sun. The solar spectrum will be directly measured when the line of sight is above the atmosphere. Thus, observations were specifically requested to build the solar spectrum over the domain accessible by the ACS-NIR spectrometer but also to study its instrumental properties and their effects on the measurements. They consisted in recording all the images of the diffraction orders of ACS-NIR by continuously varying the frequency of its acousto-optical element, the AOTF. This second objective is the aim of this paper since the first has already been studied in detail in irbah *et al.* (2022).[1] In particular, this previous paper presented the method and the different processing steps to avoid spectral contaminations between successive orders that occurs when constant AOTF frequencies are used for acquire them. This contamination is problematic in that it causes wavelengths to appear in a spectral band of a given diffraction order that actually come from its immediate neighbours. The constant AOTF frequencies are however used in the nominal mode of ACS-NIR during operations. They are chosen so that the orders are centred on the detector, i.e. in the image. The orders, however, present 2D intensity variations in particular along the x axis (wavelength) and, therefore, the spectral lines at the ends are poorly detected due to the low level of intensity. In this paper, we first recall the different processing steps to obtain the spectral bands associated with the diffraction orders. However, we have completed the original method by adding the correction of the diffraction orders of their 2D intensity variations, which improves the quality of the processing for obtaining the solar spectrum. We then present how to identify the spectral contributions of neighbouring orders to a given spectral band. Next, we present a new method that overcomes cross-order contamination by extracting two parts of images of the same diffraction order obtained with distinct AOTF frequencies. We show that this combination also brings a solution to the problem of the detection of spectral lines at the extremities where the intensity of the order is weak. Finally, we end by showing and discussing some promising results of the method obtained with the ACS-NIR order 101 taken as an example because it is likely to present spectral contamination. These results show that its neighbours no longer contaminate its spectral band. It is also of better quality compared to that calculated with the geometric method presented in the paper cited above. This method can be easily extended to all other orders, which will improve the solar spectrum obtained with ACS-NIR. It can also be used for ACS-NIR during operations without a noticeable increase in telemetry.

Keywords: Solar spectrum, Near Infrared, Mars, Spectrometer, AOTF

1. INTRODUCTION

Solar radiation is the main source of information for understanding the composition and functioning of the Sun. Its energy distribution with the wavelength defines the solar spectrum close to that of a black body at the temperature of approximately 5800 K. The black body spectrum is continuous but that of the Sun has many

Further author information: (Send correspondence to Abdanour Irbah)
A.A.A.: E-mail: air@latmos.ipsl.fr, Telephone: +33 (0)1 8028 5040

absorption lines due to the elements of the cold layer located above the photosphere which absorb the radiation coming from the layers below.[2] The solar spectrum therefore tells us about the composition of the Sun and its magnetic field, which also impacts certain solar lines. We can access the solar spectrum in different ways: using theory, calculating the solar spectrum through the Earth's atmosphere and subtracting the telluric lines like Toon[3] did, or measuring it outside of any atmosphere. The latter is the exo-atmospheric method that is used by the Near InfraRed (NIR) spectrometer of the Atmospheric Chemistry Suite (ACS) aboard the Trace Gas Orbiter (TGO) launched in 2016.[4] The ACS-NIR spectrometer having a resolving power of $\sim$ 25000 is currently being used to probe the atmosphere of Mars thanks to observations made with its nadir and Solar Occultation (SO) modes. The SO mode detects the spectral signature of atmospheric components present on the Line-Of-Sight (LOS) as it passes through the atmosphere when ACS-NIR is pointed at the Sun. The solar spectrum is then directly measured when the LOS is above the atmosphere. Specific observations were made with the ACS-NIR spectrometer to build the solar spectrum in the domain it allows, namely 0.7-1.7 µm, but also to study its instrumental properties and their effects on the measurements. These observations consisted in successively acquiring and recording series of images of all ACS-NIR diffraction orders. The specific observations were obtained by continuously varying the frequency of the ACS-NIR AOTF (Acousto-Optic Tunable Filters). The AOTF is the optical component which makes it possible to select the different diffraction orders of ACS-NIR thanks to its frequency control. They are then formed on the 2D detector and their images acquired. However, successive orders corresponding to different spectral bands can overlap leading to a *spectral contamination*. This contamination has the consequence of polluting the spectrum because it causes wavelengths to appear in the spectral band of a diffraction order which in fact come from its neighbours. Moreover, the diffraction orders present intensity variations along the x (wavelength) and y axes, which we will call *2D intensity variations* in the following. Thus, the orders correctly centred in the images have the disadvantage of having a low intensity at its ends along the wavelength axis. Indeed, the order intensity decreases from the center towards the edges because of the Blaze function of the ACS-NIR diffraction grating. The spectral lines are there with very little contrast and are difficult to detect.

The main objective of this paper is to study the spectral contamination of the diffraction orders induced by the ACS-NIR spectrometer while providing a solution to the issue of the detection of lines at the ends of the spectral bands. We will start first by presenting the ACS-NIR spectrometer as well as the observations and ancillary data used in this work. We will then continue by summarizing the different data processing steps to obtain the spectral bands associated with all the diffraction orders[1] while presenting a complement to the method based on the correction of the 2D intensity variations of the orders. We will then present how to identify the spectral contributions of neighbouring orders responsible for the contamination of a given spectral band. Next, we will show how we can overcome cross-order contamination by combining 2 parts extracted from 2 images of the same diffraction order obtained with distinct AOTF frequencies. We will show that this combination also solves the issue of spectral line detection where the order intensity is weak. We will end by showing and discussing some promising results considering the ACS-NIR diffraction order 101 likely to present a spectral contamination.

2. TGO AND THE ACS-NIR SPECTROMETER - CALIBRATION DATA AND MATRICES

2.1 The ACS-NIR spectrometer

The ACS-NIR spectrometer is a combination of an echelle spectrometer and an AOTF for diffraction order selection to achieve high spectral resolution in a compact and robust design.[4] Thus, the AOTF plays a vital role in the instrument. Its principle is based on the fact that the wavelength of the diffracted light depends on the frequency of the acoustic oscillation which crosses the crystal which composes it. The wavelength of the light wave can then be diffracted as desired by tuning the frequency of the acoustic wave. Figure 1 shows a simplified optical scheme of the ACS-NIR spectrometer to illustrate how it works. The spectrometer slit marked with the number 7 in the figure makes it possible to select only a narrow part of the solar image formed through the AOTF (numbered 4). This selected light is then diffracted by the grating (numbered 9) whose diffraction orders are formed on the detector (numbered 10). The detector is an infrared camera module XSW-640 from Xenics based on a thermo-electrically cooled (Peltier element) InGaAs array of 640 x 512 pixels. Several diffraction orders can be acquired sequentially during a measurement. They can be located anywhere in the entire spectral

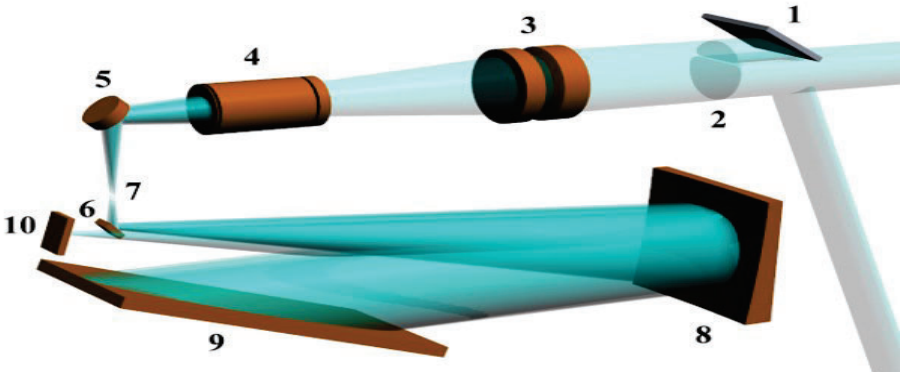

Figure 1. Optical scheme of the ACS-NIR spectrometer reproduced courtesy TGO-ACS.
1- solar FOV telescope 2- blocking filter 3- entry telescope 4- AOTF in the converging beam 5, 6- folding mirrors 7- slit 8- main collimating mirror of the spectrometer 9- diffraction grating 10- detector array

range of the instrument thanks to the frequency tuning of the AOTF. The main disadvantage of this design is the narrowness of the selected spectral intervals. In addition, side lobes of the *sinc* function representative of the AOTF spectral band-pass imply that adjacent diffraction orders superimpose on top of each other[4] resulting in a spectral contamination. Furthermore, the echelle grating efficiency quickly decreases away from the Blaze angle (centre of the detector) and, combined with a similar effect of the AOTF band-pass curve, induces a significant reduction of signal near the edges of the detector.[4] These disadvantages will lead us to special data processing to overcome them as we will see later in this paper.

2.2 The calibration data

The calibration data we are working on corresponds to the series of specific observations recorded with the ACS-NIR spectrometer when its LOS was above the Martian atmosphere. They were acquired during 3742 orbits between October 4, 2020 and August 6, 2021 (10 months). Data correspond to images of all ACS-NIR diffraction orders ranging from 45 to 103. They were obtained by continuously varying the frequency of the AOTF in steps of 100 KHz on its authorized band (64 to 156.9 MHz). For each order, we have around 16 files of 34 images, except orders 45 and 103, which have fewer files due to AOTF frequency limits: they are therefore not well defined. In total, we have 31280 images that go across the 0.7-1.7 µm spectral domain. Each of the 31280 images has 80 x 640 pixels. Indeed, only one window of the entire image of size 512×640 pixels is extracted for each diffraction order. Figure 2(a) shows a sample of a diffraction order where the solar lines are clearly visible. They are also clearly visible in Figure 2(b), which plots the slice in the image of this diffraction order passing through the ordinate of its photo-center. It shows the intensity variation of the order along the abscissa (wavelength) axis. Figure 2(c) plots also slices in this order image but passing through the photo-center (in black), at x-pixel = 100 (in red) and at x-pixel = 400 (in blue). These slices were arbitrary normalized to 1 in order to see how the order spreads out from left to right. These intensity properties along the x and y directions (2D) observed in this image generalize to all ACS-NIR diffraction orders that exhibit these same systematic 2D intensity variations. They will be taken into account when processing the data.

2.3 The calibration matrices

The flat field and stray light images of the ACS-NIR spectrometer are calibration matrices needed to correct the raw images of diffraction orders. Methods have been specially developed to estimate them since these matrices are not provided with the data to be processed.

2.3.1 The flat field calibration matrix

The flat field correction is essential to process the raw images of NIR diffraction orders. The flat field matrix will correct the intensity response of the camera pixels i.e. the pixel noise. No flat field was provided with the data

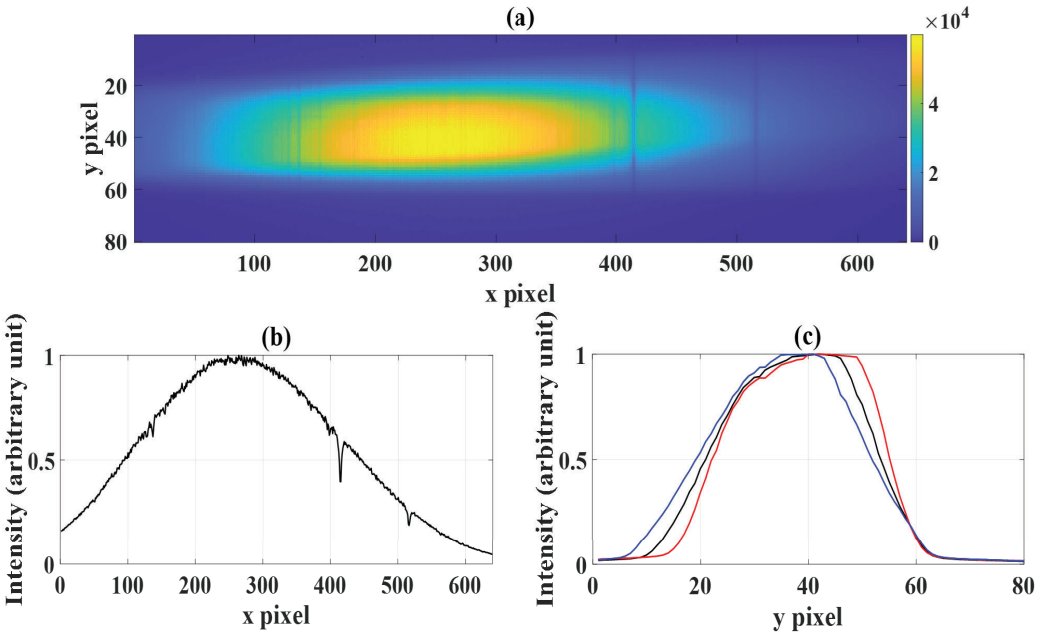

Figure 2. (a) Image of a diffraction order sample with clearly visible solar lines (Vertical dark lines). (b) and (c) show order intensity variations along the x-axis and y-axis, respectively.

so it had to be estimated. We recall here the basics of the flatfield estimation method since more details can be found in irbah *et al.* (2022).[1] The following idea was considered for its estimation directly from the calibration data. It was assumed that the average of the 31280 images (see Section 2.2) would blur the solar lines because each diffraction order image is formed on the same part of the detector and the solar lines present inside (see Fig. 2(a)) are formed at different locations from an order to the other. This average image without the traces of the solar lines will contain the flat field carried by the low frequency intensity variations along the rows and columns of the detector similar to the curves of Figures 2(b) and 2(c). However, some issues remained in the average image due to deep solar lines in some order images that were not completely blurred. They were solved by locating these solar lines and discarding them from the averaging process. At this stage, the averaged image had to be corrected for its 2D intensity variations to obtain the final flat field. The best solution found was to fit each line of the image by a polynomial of order 6. The final result is shown by the left image of Figure 3. Regarding the quality of the flat field, its analysis reveals that the standard deviation of its fluctuations is about 1.2% in the center while it is about 1.7% in the the regions where the level of intensity is weak i.e. at the edges of the diffraction order.

2.3.2 The stray light calibration matrix

The stray light matrix of the photometer was also estimated from ACS-NIR observations using the method detailed in irbah *et al.* (2022).[5] We summarize here the method developed and used for its estimation. A simulation was first carried out to explain the shape of the solar limb, that is to say the variation in intensity of the Sun along one of its diameters. The solar limbs here correspond to sections taken in the average image of the diffraction orders along the y-axis like those shown in Figure 2(c). The Hestroffer and Magnan's (H&M) solar model[6] of the centre-limb darkening function of the intensity was used to simulate images of the Sun as observed at the output of the AOTF. It is shown in the paper cited above that the AOTF is responsible for the shape of the average image of the orders shown at the top right of Figure 3 but also that the stray light can be estimated from the intensity at the bottom of the ends of the limbs. The resulting stray light image is shown at the bottom right of Figure 3. We found that the intensity level of the stray light image is about 6.7% compared to that of the average image of the diffraction orders.

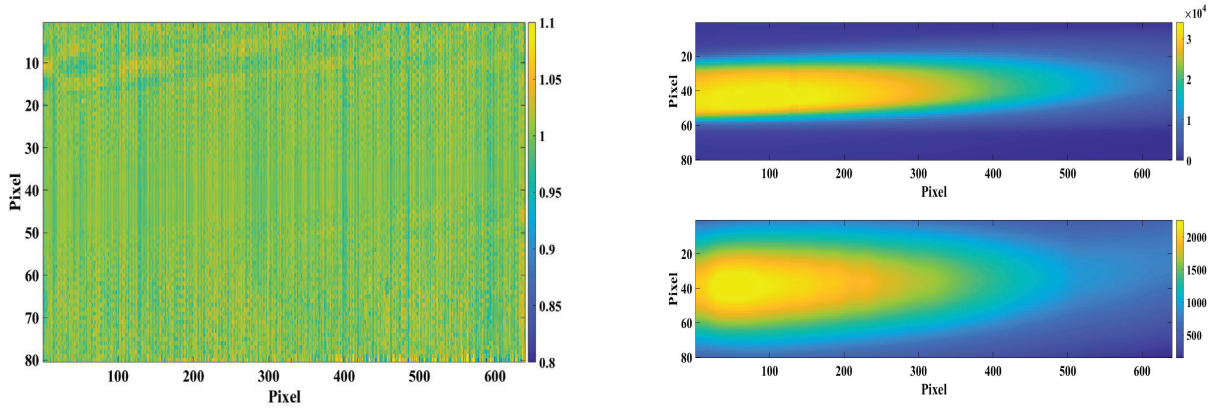

Figure 3. Left: The Flat field estimated from ACS-NIR observations. Right: The average image of all ACS-NIR orders (top) and the estimated stray light (bottom).

2.4 Spectral calibration of diffraction orders

Spectral calibration of ACS-NIR diffraction orders is possible thanks to both the grating dispersion law and a reference solar spectrum. The dispersion law expresses the relation existing between the wavelengths and the number of diffraction orders. It is written as follows:
$\lambda \cdot n = constant$ where λ and n denote respectively the wavelength and number of the order.
We first consider a given ACS-NIR diffraction order containing strong solar lines. These solar lines are identified in the laboratory or using a reference solar spectrum such as that of Toon[3,7] (see Section 2.5) as was done for the ACS-NIR Spectrometer. The identification of the solar lines then allows the spectral calibration of the diffraction order considered. A vector of 640 constants corresponding to the size of the order images along the abscissa axis is calculated from the calibrated order using the dispersion law knowing its number. The spectral calibration of all diffraction orders is immediately deduced thanks to this vector and their order number.

2.5 The solar spectrum reference: the Toon spectrum

The solar spectrum of Toon[3,7] is taken as a reference to compare that obtained with the ACS-NIR spectrometer. The solar spectrum can be obtained by various methods, including calculating it through the Earth's atmosphere and subtracting the telluric lines as Toon did. Indeed, it is a solar pseudo-transmittance spectrum calculated by fitting real spectra recorded from the ground and from balloons discriminating telluric absorption lines using the HITRAN (High Resolution Molecular Absorption) database.[8] Toon uses a telluric subtraction method to differentiate solar and telluric absorptions. It consists first of all in using a variety of solar spectra obtained under low air mass conditions and measured under different conditions (central zone or whole disk of the Sun). It then consists of adjusting the calculated telluric transmission spectrum and afterward dividing each measured spectrum by the adjusted atmospheric transmission. The solar *pseudo-transmittances* have numerical values varying between 0 and 1.[7] The upper value 1 corresponds to the solar continuum. The Toon spectrum has a very high resolution. It was therefore convoluted with a Gaussian in order to have the same resolution as the ACS-NIR spectrometer, which has a resolving power ($\frac{\lambda}{\Delta\lambda}$) of about 25000.[4]

3. PROCESSING OF ACS-NIR DIFFRACTION ORDERS TO OBTAIN THE SOLAR SPECTRUM

We presented in a recent paper[1] how to process ACS-NIR diffraction orders to extract their spectral band using a geometric method. The main stages of this processing method must first be recalled before tackling the study of order contamination.

3.1 Extraction of the order spectral bands

Consider first a diffraction order image corrected of the flat field and the stray light (see Fig. 4(a)), then define the integration region to calculate its contribution to the solar spectrum i.e. the order spectral band.

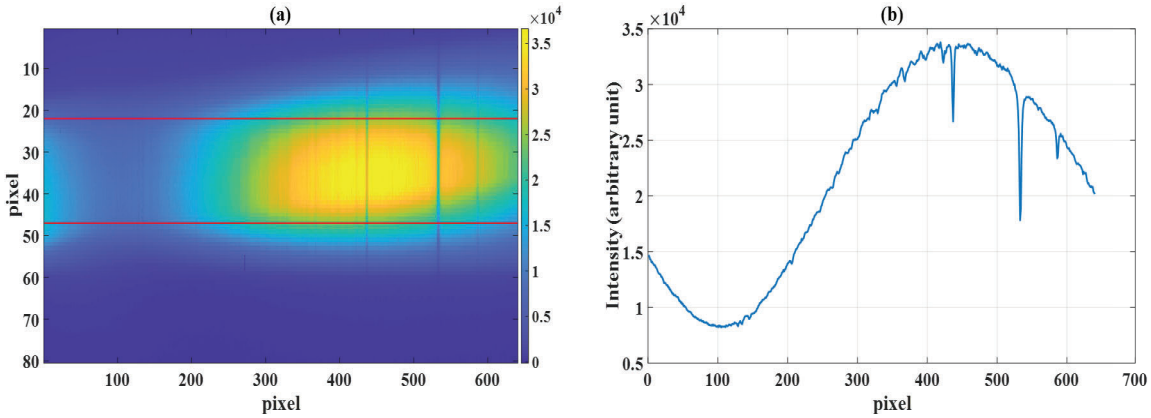

Figure 4. (a) Integration region in a diffraction order image. (b) Spectral band of the order corresponding to this integration region.

The red lines in Figure 4(a) delimit the area chosen in the image corresponding here to the whole Sun. The integration on this region of the image intensity along the y-axis corresponds to the spectral band of the diffraction order considered (see Fig. 4(b)). The solar lines carried by a low frequency variation of the continuum along the x-axis (wavelengths) are clearly visible. This process is then applied to all diffraction orders of the ACS-NIR spectrometer and the results plotted in Figure 5(a). We see that all order spectral bands have intensity variations similar like the one in Figure 4(b). We see also that the order spectral bands corresponding to the long wavelengths (small order number) are well separated whereas they overlap for the short wavelengths (large order number). This confirms the remark made on the main disadvantage of the design of the ACS-NIR spectrometer (see Section 2.1). The left part of Figure 5(a) therefore clearly shows that the successive order spectral bands are contaminated. Indeed, we recall that each order band is associated with an AOTF frequency and the contamination occurs when its value is increased to pass from one order to another. Figure 5(b) also shows all order spectral bands but as an image. Each image line corresponds to a spectral band extracted from an order associated to the AOTF frequency which made it possible to obtain it. Order 45 located at the bottom of Figure 5(b), corresponds to the low AOTF frequency while order 103 is at the top and corresponds to the high AOTF frequency. The dark spots in the image are solar lines. At this stage, we can say that we are faced with two main challenges in constructing the solar spectrum: correcting the orders for their variations in intensity and disentangling the successive orders.

3.2 Intensity correction of the spectral bands: first approach

A new method was developed for the correction of 2D intensity variations of the orders. The solution implemented is to extract the envelope defining the global intensity of each order image without the solar lines, then to correct the original image of this envelope. The first step is therefore to locate the solar lines in the order images. For this, a few lines in the center of the order image are averaged (see blue curve in Fig. 6) and the local maxima along the averaged line are detected (red dots in Fig. 6). The typical order 59 taken to illustrate the process is shown at the top left of Figure 7. The local maxima are globally located at the beginning and at the end of each solar line. The local maxima are therefore considered as parts of the envelope of the signal and the whole envelope is obtained by interpolating all the other points. A threshold is defined to detect the solar lines and all the points which are below with respect to the envelope are solar lines. We have at this stage the abscissa of the solar lines and we can interpolate them in the image. To improve the cleaning operation of solar lines, the image is resized to a smaller size before resizing it to its initial size (80 x 640 pixels). Thanks to this second processing pass, The solar lines are completely erased as seen in the top-right image of Figure 7. A few "NaN" (Not a Number) pixels appear at the top right of the image after resizing, but this has no consequences because the areas of interest for obtaining the solar spectrum are located in the center of the image. The last step consists in correcting the order image of its intensity variations by dividing it by its envelope (bottom image of Figure 7). The process of the 2D intensity correction is then applied to all ACS-NIR orders and the result is shown in

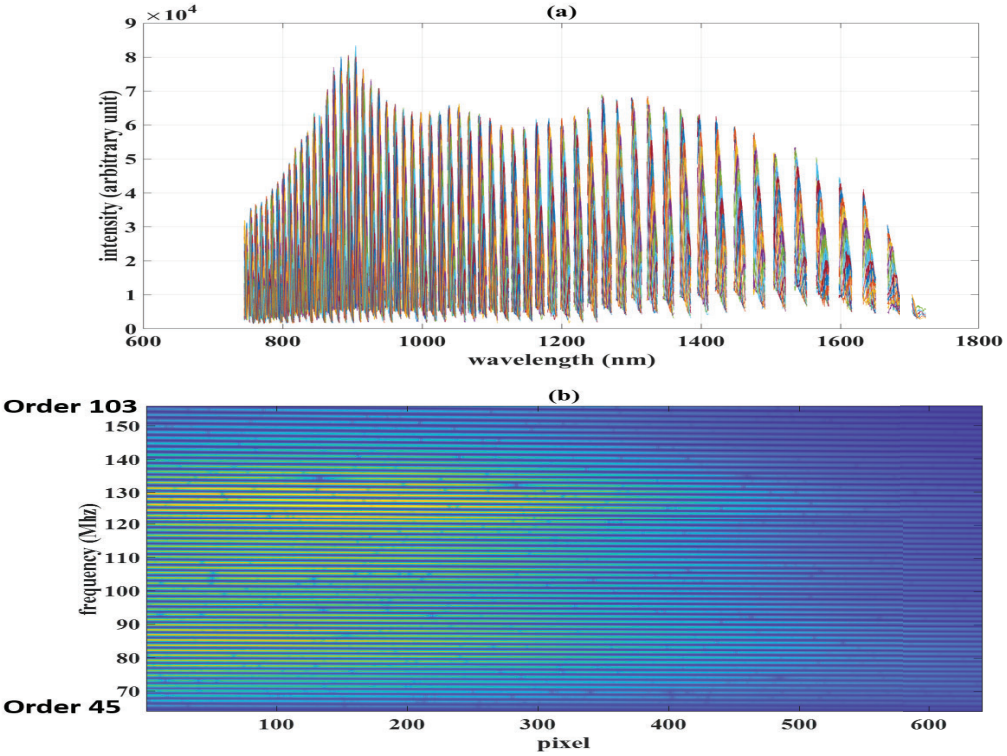

Figure 5. (a) All ACS-NIR spectral bands extracted from order images when varying AOTF frequency as a function of wavelength: they are affected by large intensity variations. (b) The same spectral bands as (a) but shown as an image: each spectral band is associated with its AOTF frequency and its order number.

Figure 8. Figure 8(a) shows all the spectral order bands corrected to the first order of intensity variations. The spectrum that we obtain is now close to the final one, with a continuum around 1. We can clearly see the order contamination for short wavelengths as highlighted in Section 3.1 for Figure 5. A second process will be used to correct for residual intensity variations as was done in the previous work.[1] Figure 8(b) also shows all spectral

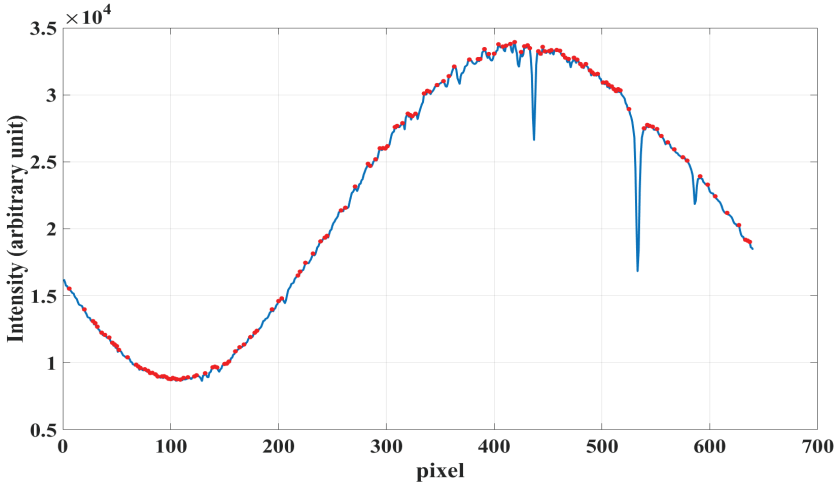

Figure 6. Detection of local maxima (red dots) on the average of a few lines (blue curve) taken in the image center of order 59 taken as example.

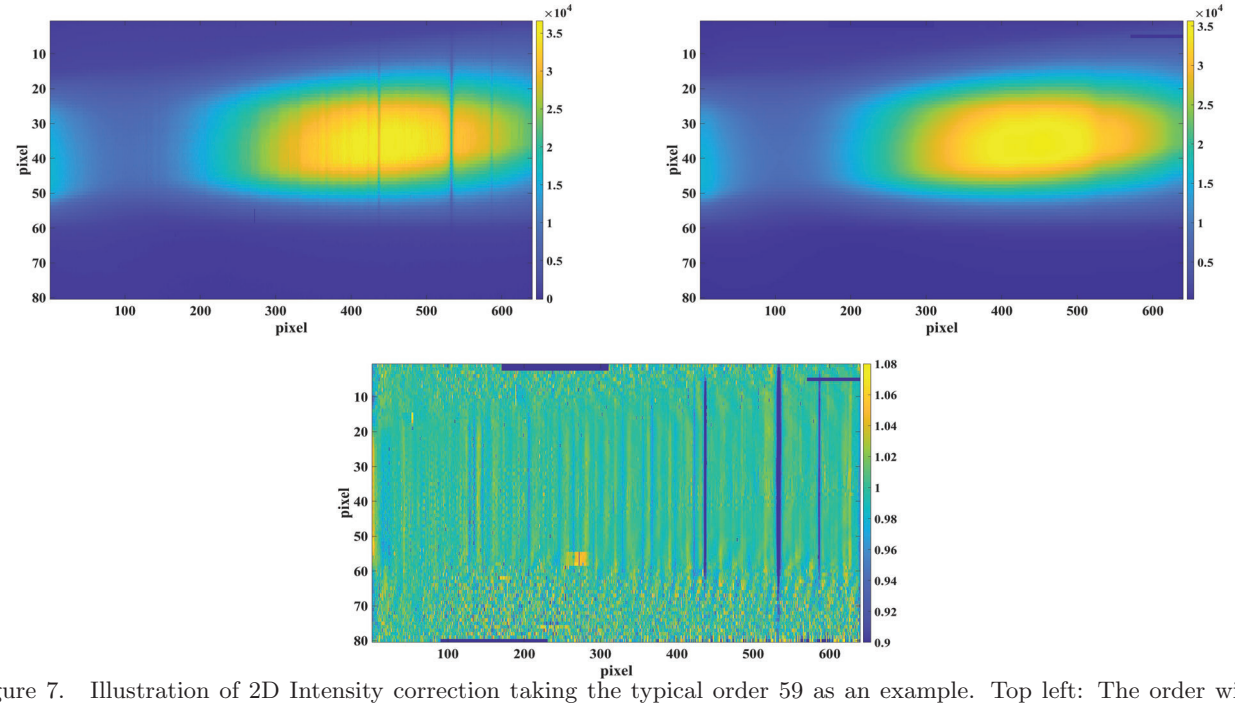

Figure 7. Illustration of 2D Intensity correction taking the typical order 59 as an example. Top left: The order with visible solar lines. Top right: The same order without solar lines. Bottom: Order corrected from intensity variations

bands as in Figure 5(b). Each image line corresponds to a spectral band extracted from an order associated with its AOTF frequency. The dark spots correspond to the solar lines.

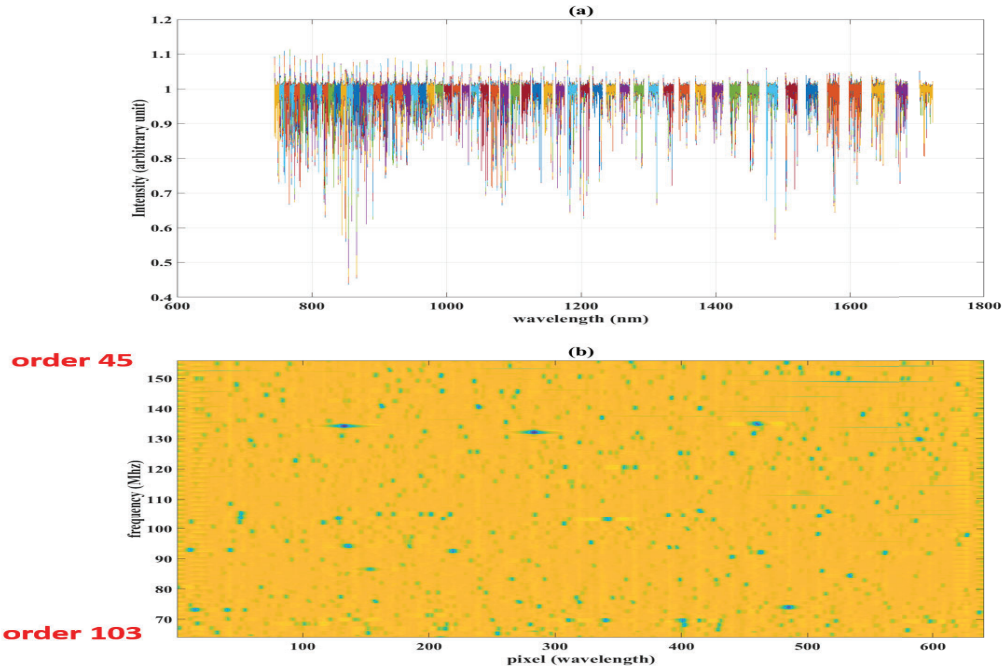

Figure 8. All ACS-NIR spectral bands extracted from order images when varying the AOTF frequency as a function of wavelength (a) and shown as an image (b): they are corrected from 2D intensity variations.

3.3 Processing of diffraction orders

As mentioned in Section 3.1, the next issue to solve is the disentanglement of diffraction orders. For this and to fully understand the problem, we can zoom in on the image of Figure 5. We can thus observe at the top left of Figure 9 which is a zoom in the image that two or more orders are involved by the same AOTF frequency represented by horizontal white lines in the figure. Thus, one or more same wavelengths can be present in several spectral bands (see top right of Fig. 9). Indeed, the diffraction orders are tilted when they are represented in the frame (AOTF frequency , Detector column). Thus, the solar spectrum will be polluted by the same wavelengths,

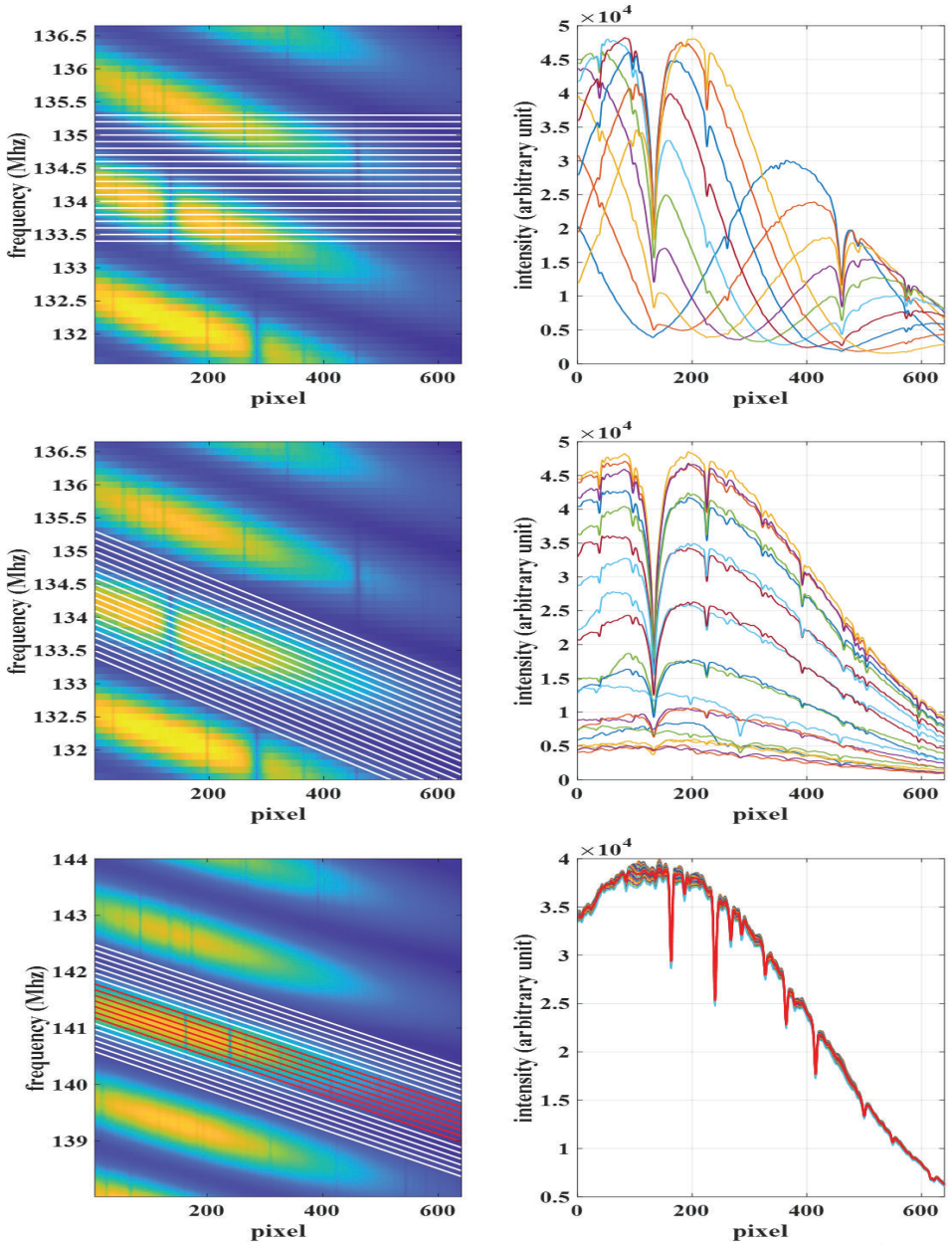

Figure 9. Top: Diffraction order 90 and extracted horizontal slices corresponding to constant AOTF frequencies (white lines). The corresponding intensity profiles of image slices are plotted in the right panel. Middle: Diffraction order 90 and extracted oblique sections corresponding to varying AOTF frequencies (white lines). The corresponding intensity profiles of image slices are plotted in the right panel. Bottom: Spectral band extracted from diffraction order 94 (red lines on the left) and the intensity variation along the pixel axis on the right The red curve is the average of these intensity profiles.

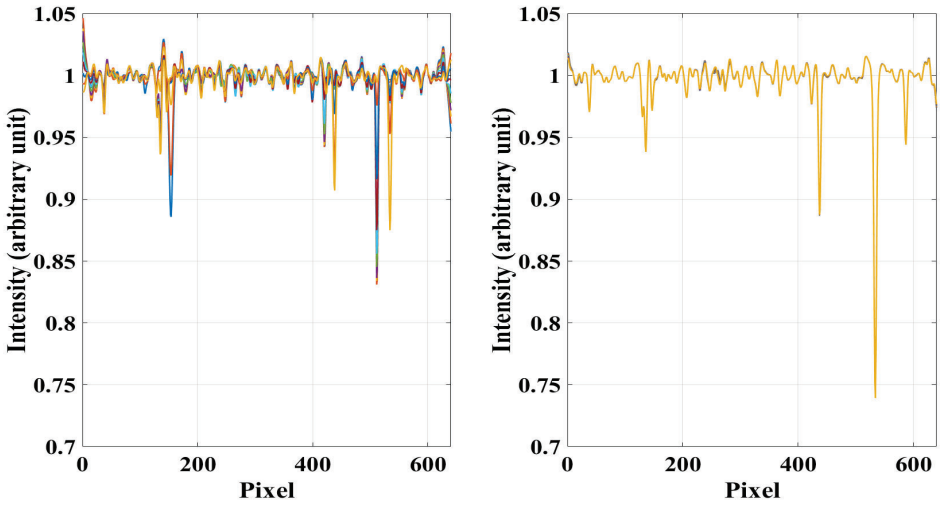

Figure 10. Comparison between horizontal (left) and oblique (right) cuts using the spectral band image corrected of the 2D intensity variations in case of order 59.

which will appear there in several places if the spectrum is directly constructed from horizontal slices taken in this frame. The solution is then to take oblique slices in the image of Figure 5 following the inclination of the order as shown in the middle left of Figure 9. Tilt is first calculated by linearly joining the intensity maxima in the first column of the image with its counterparts in the last column (index 640). Slices in the image are then made along this direction as shown in the middle right of Figure 9 where we can see that all the wavelengths are in their correct locations for the order considered. For each order, we finally select a few slices around the maximum intensity to avoid contamination of neighbouring orders (red lines in bottom left of Figure 9). The last step consists in calculating the average of these slices, thus obtaining the spectral contribution of the diffraction order to the solar spectrum (red curve in bottom right of Figure 9). The intensity variation along the pixel (wavelength) axis is clearly visible as expected. We have shown in irbah *et al.* (2022)[1] that the intensity variation is well adjusted with a Blaze function which is then used to correct it. Here we can directly use the image of the intensity-corrected spectral bands (see Fig. 8) and apply the oblique cutting process described above. Figure 10 plots the results obtained for order 59 by considering horizontal (left curves) and oblique (right curves) slices in the image. It can be noted in this last case that all the curves have the same shape, proving that all the wavelengths are well localized for the order considered. Compared to the case where the images are not corrected for 2D intensity variations, the resulting spectra no longer have the intensity varying according to a Blaze function and it is no longer necessary to make this correction. The next and final step is the continuum enhancement set arbitrary to 1 using the same process as described in irbah *et al.* (2022).[1] In short, it consists in calculating the local maxima of the averaged spectrum then in using them to create an interpolation function at each point of this spectrum and finally in correcting it by this function. For each order, the average of the spectra obtained with the oblique cuts is calculated and the continuous improvement process applied.

3.4 The solar spectrum

The processing chain was applied to the 59 diffraction orders of the ACS-NIR spectrometer to calculate the solar spectrum over the 0.7-1.7 µm domain in the case where the whole Sun is considered (see Section 3.1). We get what is shown at the top in Figure 11 where the black curve represents the final solar spectrum obtained from ACS-NIR. The green curve corresponds to the Toon solar spectrum, which is our reference (see Section 2.5) for comparison. We see that the 2 spectra are very close except for the depth of the solar lines which is different but expected since ACS-NIR is not a spectroradiometer. Thus, we will therefore only be interested in the spectral content that ACS-NIR makes it possible to recover. The bottom plot in Figure 11 zooms in on the 2 spectra at

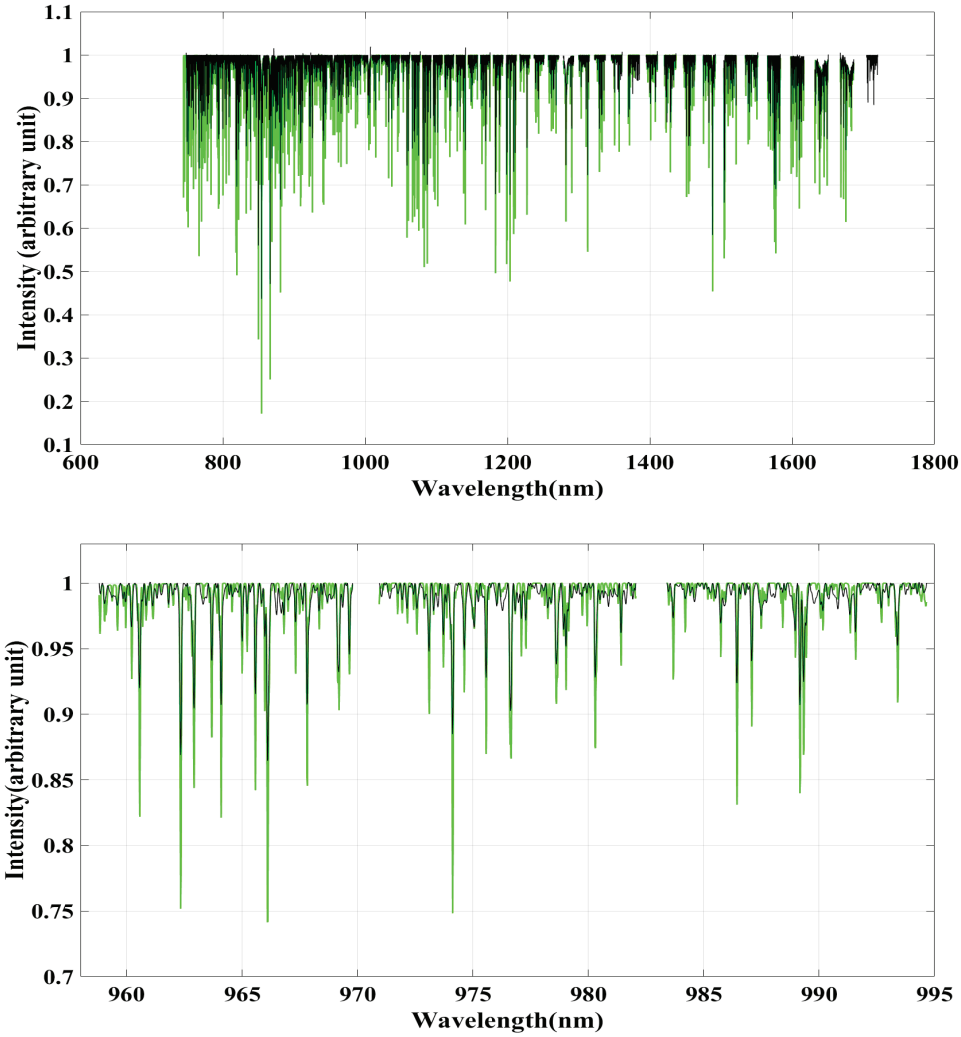

Figure 11. Top: Final ACS-NIR solar spectrum (black) with the Toon reference spectrum (green). Bottom: Good agreement observed between the ACS-NIR (black) and Toon (green) solar spectra when zooming in closer on orders 80, 79 and 78.

particular diffraction orders 80, 79 and 78 (from left to right) to see a closer comparison with the Toon spectrum. This confirms the fairly good agreement between the 2 spectra but also the previous remark on the difference in depth of the solar lines. Some details in the continuum of the two spectra are also highlighted.

4. STUDY OF THE ORDER CONTAMINATION

At this stage, we can conclude that we are able to reconstruct the solar spectrum from the calibration data specifically acquired with the ACS-NIR spectrometer. ACS-NIR observations made in nominal operating mode to probe the Martian atmosphere require the acquisition of chosen diffraction orders related to constant AOTF frequencies. This can therefore result in spectral contamination between adjacent orders which can be problematic in particular in the case of the acquisition of diffraction orders having high numbers. This section presents a study of the spectral contamination between orders. It is made possible thanks to the work presented in the previous section which allows to reconstruct the uncontaminated solar spectrum with the ACS-NIR spectrometer.

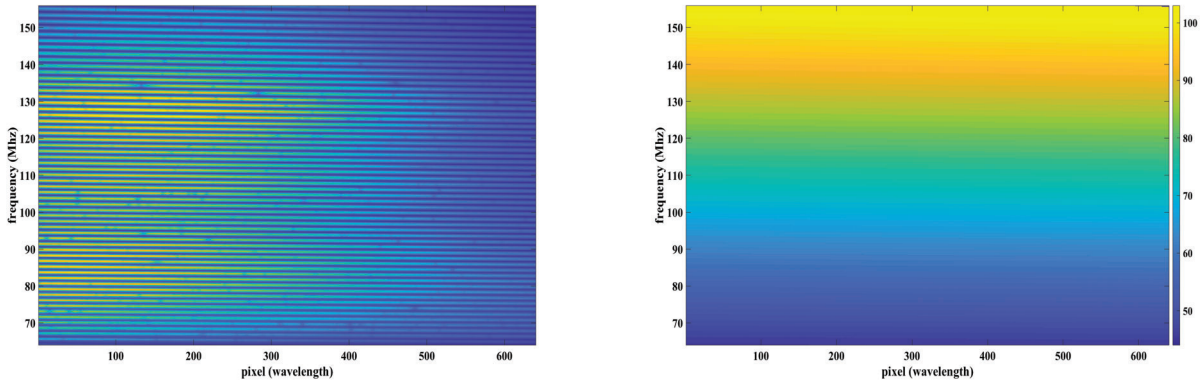

Figure 12. Left: All ACS-NIR spectral bands uncorrected for 2D intensity variations extracted from order images obtained by varying the AOTF frequency. Right: coding of the spectral bands with their order numbers.

4.1 The order contamination study

The main idea for the study of contamination between adjacent orders is first to encode each spectral band with its diffraction order number. The left image in Figure 12 shows all ACS-NIR spectral bands obtained as explained in Section 3 and their coding with the respective order numbers ranging from 45 to 103 (right image). The uncorrected spectral bands of the 2D intensity variations make it easier to find the limits of each order associated with the AOTF frequency by searching for the intensity extrema along the y axis. A zoom on the two images of Figure 12 around order 101 with 2 adjacent orders on either side is represented on the images at the top left and bottom of the Figure 13 where we see well the coding of diffraction orders. We will use in the following, once the coding has been carried out first, the image of the spectral bands corrected for 2D intensity variations as shown in Figure 13 at the top right.

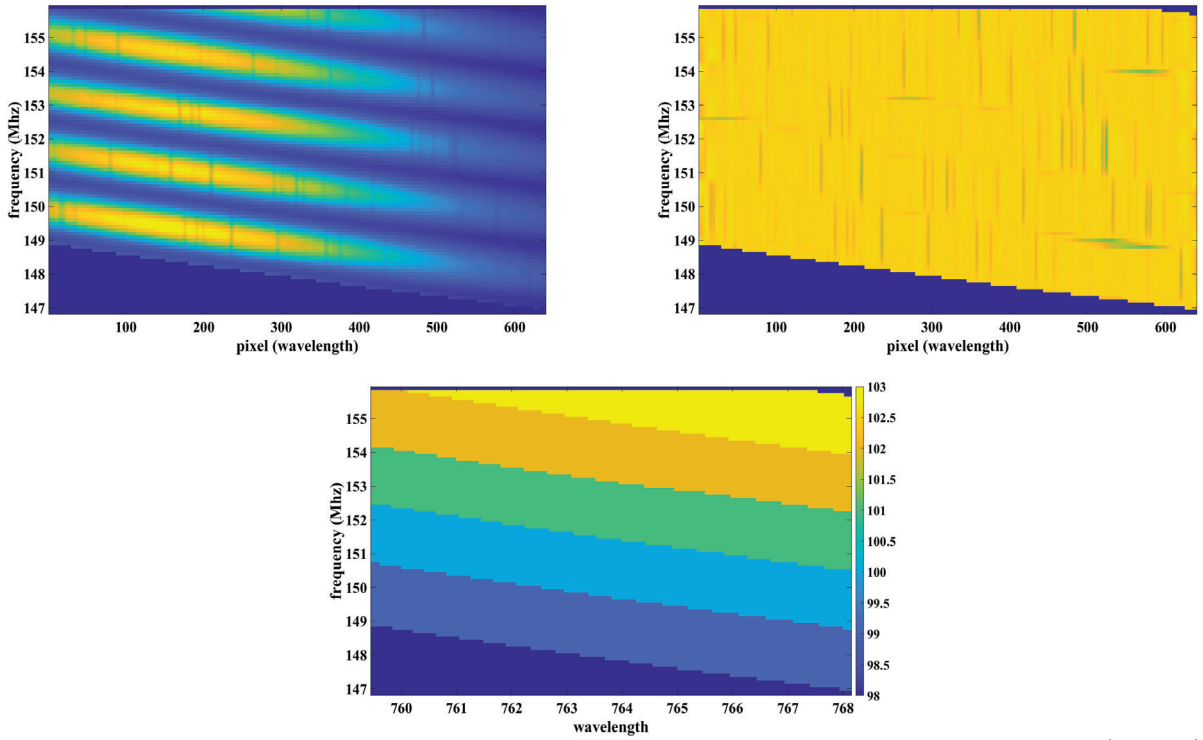

Figure 13. Some successive diffraction orders around order 101 and their coding with their numbers (*see text*).

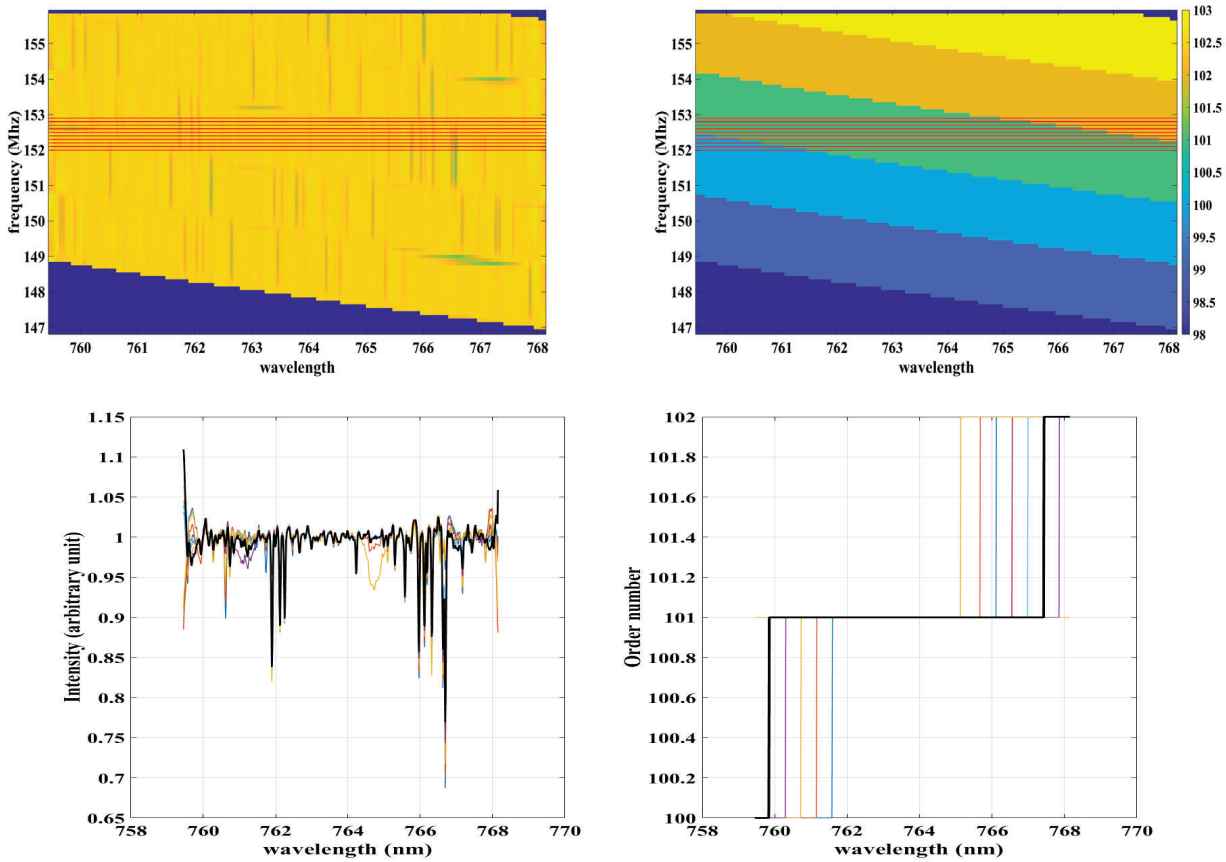

Figure 14. Top: Constant AOTF frequencies (red lines) on the images of the spectral bands (left) and coded orders (right) of order 101 with 2 adjacent orders on either side. Bottom: Profiles in images corresponding to constant AOTF frequencies (left) and impacted orders (right). The dark line corresponds to the AOTF frequency that minimizes order contamination.

An order with a high number where the entanglement between orders is clearly visible (order 101 for example, see Section 3.1) is considered to study spectral contamination. It is expected to be present when constant AOTF frequencies are taken for the acquisition of diffraction orders, especially for those with a high number. We then first consider horizontal slices in the image of the spectral bands corrected for 2D intensity variations as shown by the red lines in the image at the top left of Figure 14 which corresponds to order 101 and 2 adjacent orders on each side. These horizontal slices corresponding to constant AOTF frequencies are also represented by red lines in the coded image of the diffraction orders considered (top right of Figure 14). It is clearly seen in this figure that the same line (i.e. at constant AOTF frequency) crossing order 101 also intercepts diffraction orders 100 and 102 as shown in Figure 14 bottom right where the profiles taken from the coded image along the red horizontal lines are plotted. The dark line is the AOTF frequency which minimizes the inter-order contamination which is well visible at the ends of the spectral band. Indeed, this frequency is the one among all which gives the maximum number of pixels which define the order considered (here 101) and the minimum in the adjacent orders (here 100 and 102). The plot at the bottom left of Figure 14 shows the spectral bands corresponding to constant AOTF frequencies where the black line is also that of least contamination. The two figures at the bottom clearly show the entanglement of the orders and consequently of the wavelengths of the solar lines, which was highlighted in Section 3.3.

Knowledge of the true spectral band is essential to correctly judge the contamination of the order 101. For this, the geometric method summarized in Section 3.3 and which consists of taking oblique slices in the image of the spectral bands corrected for 2D intensity variations, is used. The top left image of Figure 15 shows the oblique slices taken in this spectral band image following the AOTF frequency drift with wavelength. We can therefore

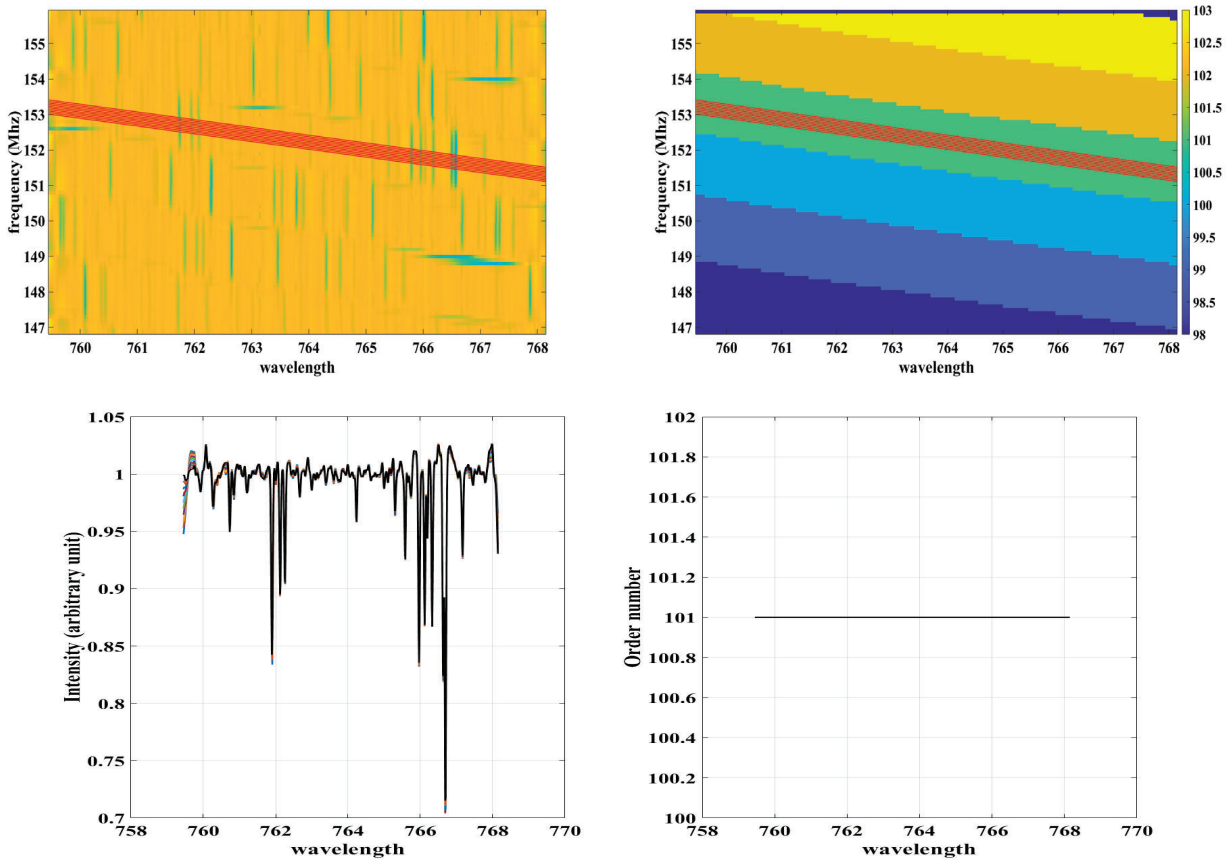

Figure 15. Top: Oblique slices following AOTF frequency drift with wavelength (red lines) shown on images of spectral bands (left) and coded orders (right) but limited to order 101 and adjacent order 2 on each side: only order 101 is involved. Bottom: Spectral bands corresponding to the profiles of the oblique slices (on the left) and of the orders concerned (only 101) (on the right).

see that these slices are all taken in the same order (101) (see top and bottom right in Figure 15) and that the corresponding spectral bands have the same shape as expected (see bottom left in Figure 15), i.e. the solar line wavelengths are in their correct location.

The last step consists in improving the continuum (see Section 3.3) of the spectral band of least contamination corresponding to the optimal AOTF frequency (its value is 152.35 MHz for order 101) but also that of the average shape of the spectral bands obtained from the different oblique slices (see bottom left in Figure 15). Figures 16(a) and (b) respectively plot the final spectral band extracted from order 101 in case of oblique slices and constant AOTF frequency. The Toon reference spectrum is also plotted in green on each spectrum for comparison. It can be noted that the spectral band obtained from the geometric method is very close to the reference whereas there are some differences with that obtained with the constant AOTF frequency. These differences are mainly at the ends of the spectral band where contamination occurs as already mentioned before. Figure 16(c) also plots the spectral band of order 101 in the case of a constant AOTF frequency but obtained from spectral band image not corrected for 2D intensity variations. It can be seen that the image of diffraction order 101 is centred on the detector and that the intensity at the ends is weak. This low level of intensity will have the consequence that the solar lines will be poorly detected at the extremities, in addition to the effects of contamination by the adjacent diffraction orders.

We will see in the next section how to overcome both the contamination between adjacent diffraction orders and the low level of intensity at the ends of the orders leading to poor detection of the solar lines at these locations.

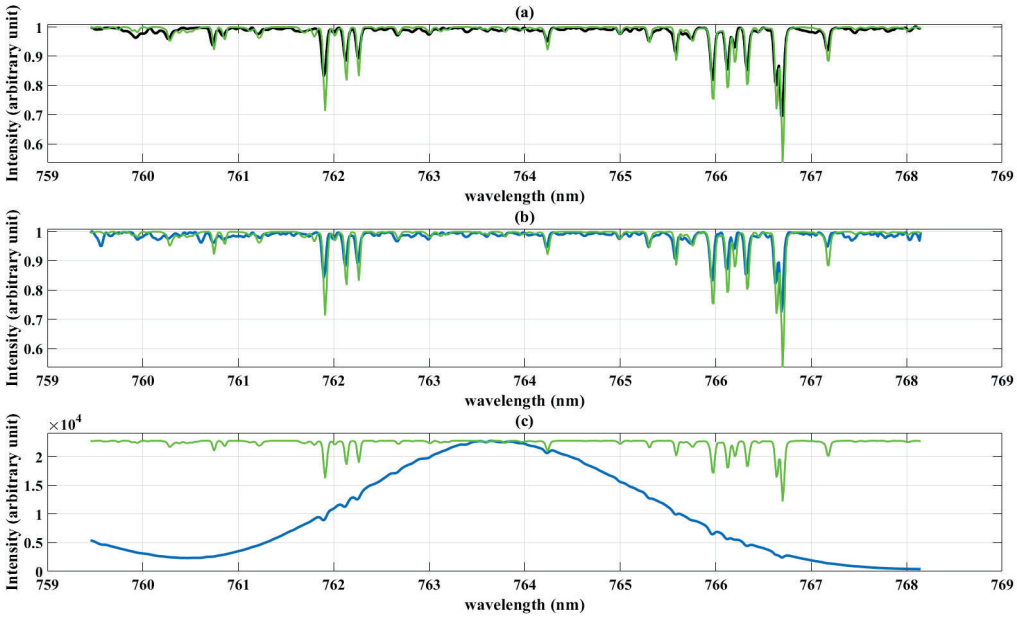

Figure 16. Spectral band of diffraction order 101 obtained with oblique (a) and horizontal (b) slices in the spectral band image corrected for 2D intensity variations. (c) is the same as (b) when slices are taken in the uncorrected spectral band image of 2D intensity variations. The Toon reference spectrum is plotted in green.

4.2 How obtaining order spectral bands without contamination

The solution proposed to overcome spectral contamination between adjacent orders must be valid during operations, i.e. for observations in nominal mode of the ACS-NIR spectrometer. It is in fact not possible to always vary the AOTF frequency continuously to apply the geometric method summarized earlier in this article. Indeed, the authorized telemetry level of the nominal mode is low and consequently only a few lines of images of a given order are acquired by means of a few AOTF frequencies.

We also use here the calibration data to carry out the spectral contamination study leading to a solution which is free from it. Indeed, these data have the advantage of containing information on the evolution of a given diffraction order, that is to say to follow the transition between an order and its next when the AOTF frequency varies continuously in step of 0.1 MHz (see Section 2.2). Thus, any given diffraction order will begin to appear at some AOTF frequency related to it, resulting in its truncated image on the detector. As the AOTF frequency increases, it will reach its maximum size where its image will be complete and centred on the detector. Finally, it will begin its decay to end again in a truncated image on the detector but formed opposite to that which saw its birth. In the nominal mode used to probe the Martian atmosphere, the AOTF frequency is taken so as to form the image of the diffraction order centred on the detector. For example, the AOTF frequency for the acquisition of order 101 in nominal mode is 152.35 MHz and it is most likely contaminated by its neighbours as explained in the previous section. It is the same for the acquisition of orders with high numbers, that is to say the orders corresponding to short wavelengths (see previous section). The idea here to avoid contamination is to take two or three incomplete images of the considered diffraction order then to recombine them to reconstruct its associated spectral band. Figure 17 shows two diffraction order images selected to construct the spectral band of order 101 which is again taken as an example to illustrate the method. These images shown respectively in the upper and lower panels of the figure were obtained with the 2 AOTF frequencies 153 and 152.1 MHz. The image of the order acquired at the 153 MHz frequency will be used to construct the left part of the spectral band while the other at 152.1 MHz for the right part. This is well illustrated in Figure 18(a) where the spectral band of the image acquired at 153 MHz is plotted in red and that acquired at 152.1 MHz in green. They were calculated by considering the uncorrected order images of 2D intensity variations (see Section 3.2) and the whole Sun was taken

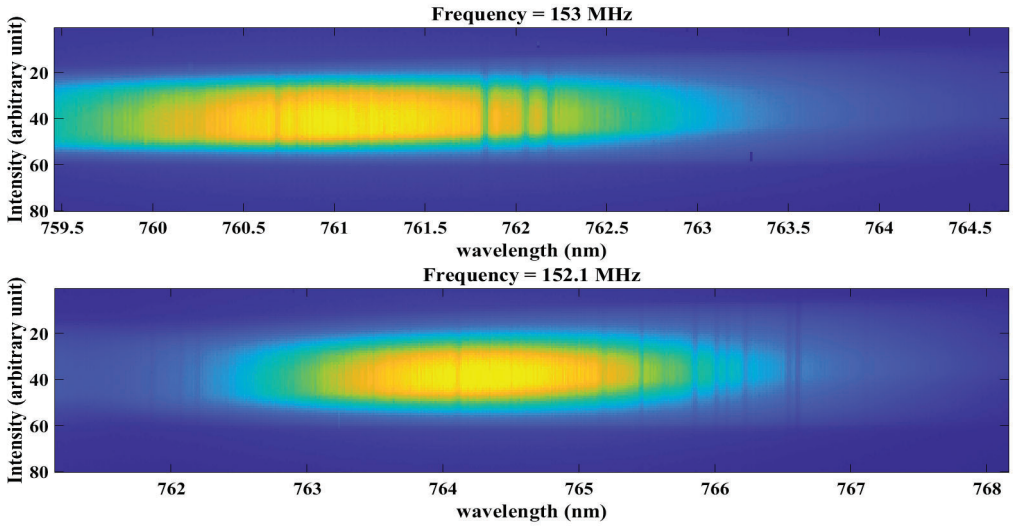

Figure 17. Truncated images of the same diffraction order (101) which will be used to build its spectral band.

as the integration region (see Section 3.1). We can see in Figure 18(a) that the intensity level at the beginning of the red curve is high which will help to better define the solar lines in this region compared to the nominal case where the intensity level is lower at the extremities. This is unfortunately not the case for the end of the green curve corresponding to the second part of the spectral band of the order where the improvement will be little perceptible. A simple way to provide a solution if necessary would be to take a second more off-center image or even three parts of images of the same order instead of two. The next step is to calculate the x coordinate (wavelength) of the intersection of the red and green curves. The combined curve is the assembly of the left curve (red) until this intersection with the right curve (green) which starts from the intersection. The result is plotted in black in Figure 18(a). Figure 18(b) shows the same curves as (a) but obtained from order images corrected for 2D intensity variations (see Section 3.2). Once this processing is done, the last step is to improve the continuum

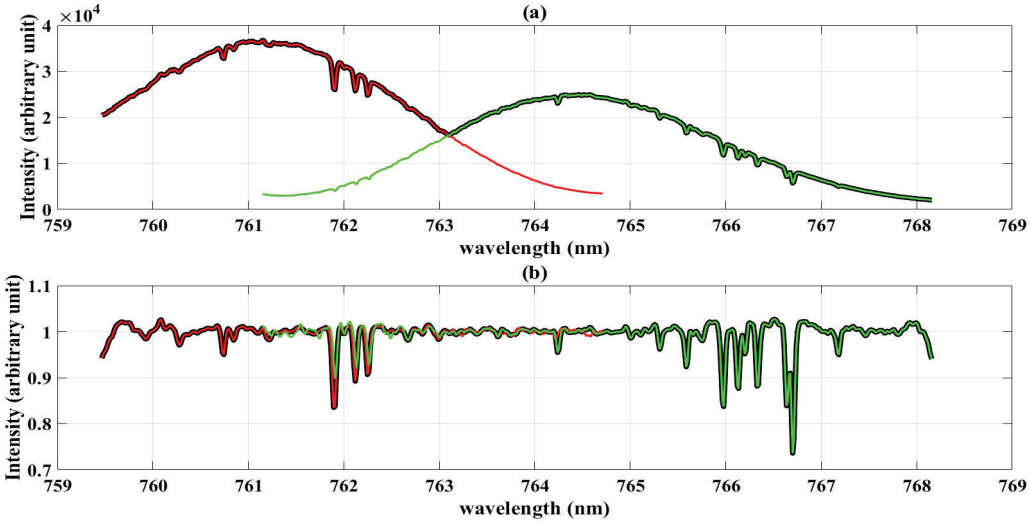

Figure 18. Spectral bands obtained from images of diffraction order 101 without (a) and with (b) correction for 2D intensity variations: they are then combined to obtain the uncontaminated spectral band of order 101.

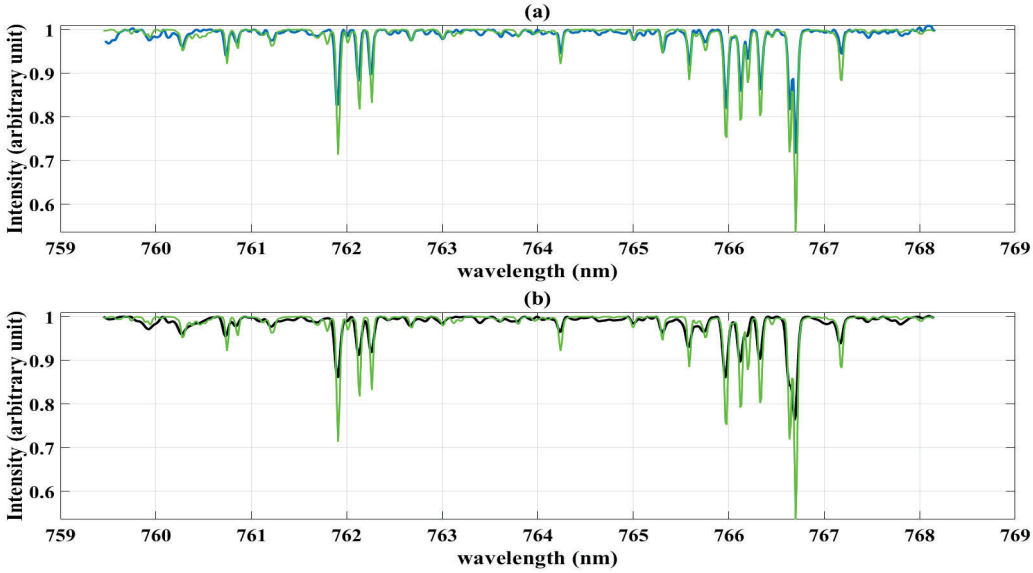

Figure 19. Spectral band of diffraction order 101 obtained from the combination of 2 images of this order (a) and from oblique slices in the image of the spectral bands corrected for 2D intensity variations (b). Toon's spectrum is in green.

of the combined spectral band as explained in Section 3.3. Figure 19(a) plots the final result of the combined spectral band of order 101 (blue curve) as well as Toon's reference spectrum for comparison (green curve). A very good agreement is observed between the two spectra. No additional solar lines due to contamination are observed at the ends of the spectral band. Figure 19(b) also plots the same spectral band but obtained from orders corrected for 2D intensity variations and the oblique cut process (black curve). The Toon spectrum is also plotted in green. We have very similar results obtained with the 2 methods, the combination of order images and the geometric method. These 2 spectra are moreover represented in Figure 20 for a better comparison. We see in this figure that the spectrum resulting from the combination of the 2 images of the order gives better results. Indeed, we can notice that the solar lines are deeper but also better resolved (see part of the spectrum between 766 and 767 nm). Finally, the spectral band resulting from the combination of the images (blue curve) and that

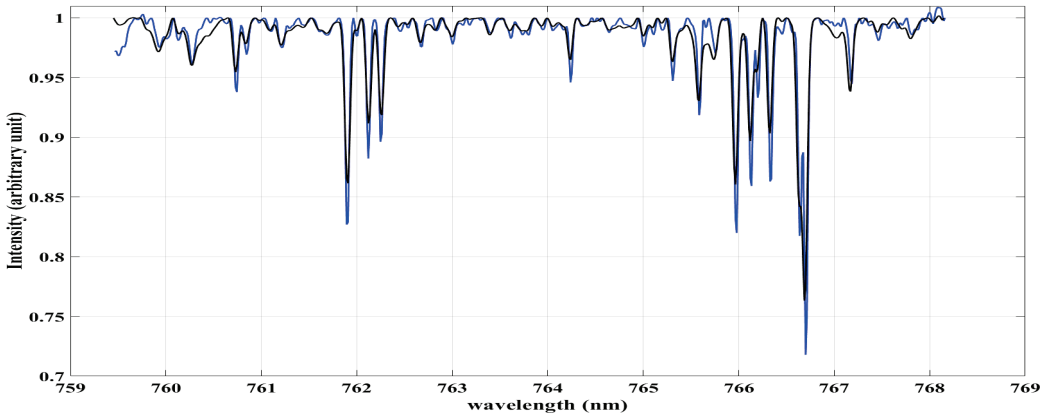

Figure 20. Spectral band of diffraction order 101 obtained from the combination of 2 images of this order (blue curve) and oblique slices in the image of spectral bands corrected for 2D intensity variations (black curve).

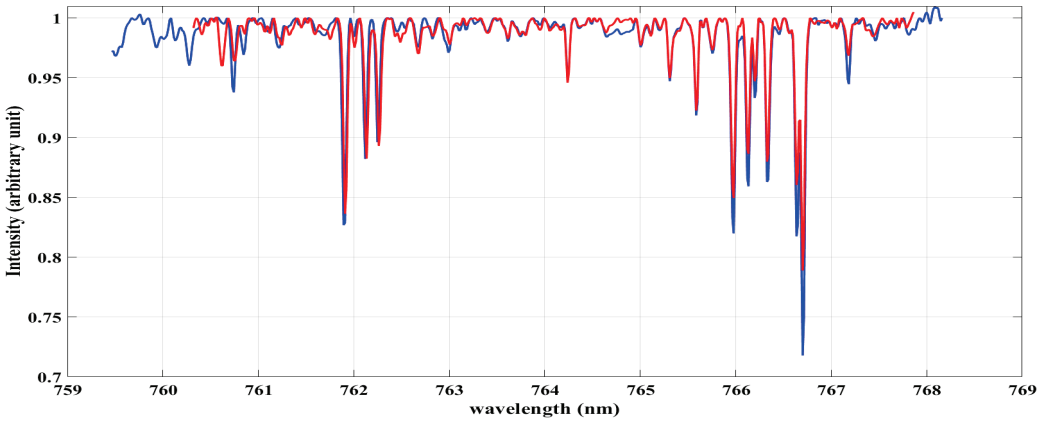

Figure 21. Spectral band of diffraction order 101 of the nominal mode (red) and obtained from the combination of 2 off-center images of the same order (blue).

obtained from the nominal mode (red curve) are plotted in Figure 21 for comparison. We see in the figure that there is a notable difference at the ends of the spectral band, in particular on the left but also in the depth of the solar lines. Moreover, the spectral band is wider in the case where the combination of images of the order is used compared to that of the nominal mode. This is due to the fact that we use 2 images of the same order which have different lower and upper AOTF frequency limits compared to those of the nominal mode.

5. CONCLUSION

Knowledge of the solar spectrum at high spectral resolution is fundamental for the study of the star itself or for space missions probing the atmosphere of planets (Earth, Mars, etc.). Indeed, it is essential for the calibration of atmospheric spectra measured by instruments such as the ACS-NIR spectrometer on board the TGO space mission in orbit around Mars since 2016. The measurement of the solar spectrum can be obtained with this spectrometer when pointed at the Sun and its line of sight is above the atmosphere. Specific observations were therefore made for this purpose but also to study the effects of instrumental properties of the ACS-NIR spectrometer on the measurements. The first objective has already been the subject of a first study detailing a geometric method adapted to the specific observations for obtaining the solar spectrum.[1] The second objective is therefore the subject of interest of this work. Indeed, the observations in the nominal mode of the ACS-NIR spectrometer during operations impose well-chosen constant AOTF frequencies to acquire the desired diffraction orders. It was then necessary to know the consequences of these choices on the spectral bands associated with the chosen orders of diffraction, namely its spectral contamination by the adjacent orders. This contamination has the consequence of polluting the spectrum by causing wavelengths to appear in the spectral band of a diffraction order which in fact come from its neighbours. In addition, an order centred in the image such as that acquired in nominal mode presents 2D intensity variations in particular along the x axis (wavelength) and consequently the spectral lines at the ends will be poorly detected due to low intensity level. This paper therefore aims to study the spectral contamination of the diffraction orders induced by the ACS-NIR spectrometer while providing a solution to the issue of detecting lines at the ends of the spectral bands. We first presented the ACS-NIR spectrometer as well as the observations and ancillary data used in this work. We then continued by summarizing the different data processing steps of the geometric method which makes it possible to obtain the spectral bands associated with the diffraction orders. However, we have completed the original processing method by first correcting the diffraction orders of the 2D intensity variations, which improves the processing, in particular the quality of the obtained spectra. We then presented how to identify the spectral contributions of adjacent orders responsible for the contamination of a spectral band of a given order. We have thus proposed a method that overcomes cross-order contamination by combining 2 parts extracted from 2 images of the same diffraction order obtained with distinct AOTF frequencies. We have shown that this combination also brings a solution to the issue of the

detection of spectral lines where the intensity at the order ends is weak. This method can easily be extended to using 3 images of the same order if desired. We then finished by showing and discussing some promising results of the method, considering the ACS-NIR order 101 likely to exhibit spectral contamination. These results showed that the spectral band obtained is no longer contaminated by its neighbours but that in addition it is of better quality compared to that calculated with the geometric method presented in the previous article[1] or even compared to that obtained from nominal mode. This method can easily be extended to all other orders, which will improve the solar spectrum obtained with ACS-NIR. It can also be used for the nominal mode of the ACS-NIR spectrometer during operations without a noticeable increase in telemetry.

REFERENCES

[1] Irbah, A., Bertaux, J.-L., Montmessin, F., Scheveiler, L., Lacombe, G., Trokhimovskiy, A., Korablev, O., Fedorova, A., Patrakeev, A., and Shakun, A., "Processing of ACS-NIR observations to build the solar spectrum with high spectral resolution in the 0.7-1.7 µm domain," in [*Space Telescopes and Instrumentation 2022: Optical, Infrared, and Millimeter Wave*], Coyle, L. E., Matsuura, S., and Perrin, M. D., eds., **12180**, 121803H, International Society for Optics and Photonics, SPIE (2022).

[2] Vial, J.-C., [*1. Le Soleil, une étoile dans notre Galaxie In : Le ciel à découvert [inline]*], Paris : CNRS Éditions (2010).

[3] Toon, G. C., "Solar line list for the tccon 2014 data release," (2015).

[4] Korablev, O., Montmessin, F., Trokhimovskiy, A., Fedorova, A., Shakun, A., Grigoriev, A., Moshkin, B., Ignatiev, N., Forget, F., Lefèvre, F., Anufreychik, K., Dzuban, I., Ivanov, Y., Kalinnikov, Y., Kozlova, T., Kungurov, A., Makarov, V., Martynovich, F., Maslov, I., Merzlyakov, D., Moiseev, P., Nikolskiy, Y., Patrakeev, A., Patsaev, D., Santos-Skripko, A., Sazonov, O., Semena, N., Semenov, A., Shashkin, V., Sidorov, A., Stepanov, A., Stupin, I., Timonin, D., Titov, A., Viktorov, A., Zharkov, A., Altieri, F., Arnold, G., Belyaev, D., Bertaux, J., Betsis, D., Duxbury, N., Encrenaz, T., Fouchet, T., Gérard, J., Grassi, D., Guerlet, S., Hartogh, P., Kasaba, Y., Khatuntsev, I., Krasnopolsky, V., Kuzmin, R., Lellouch, E., Lopez-Valverde, M., Luginin, M., Määttänen, A., Marcq, E., Torres, J., Medvedev, A., Millour, E., Olsen, K., Patel, M., Quantin-Nataf, C., Rodin, A., Shematovich, V., Thomas, I., Thomas, N., Vazquez, L., Vincendon, M., Wilquet, V., Wilson, C., Zasova, L., Zelenyi, L., and Zorzano, M., "The atmospheric chemistry suite (acs) of three spectrometers for the exomars 2016 trace gas orbiter," *Space Science Reviews* **214**(1) (2018).

[5] Irbah, A., Bertaux, J.-L., Montmessin, F., Scheveiler, L., Rouanet, N., Trokhimovskiy, A., Korablev, O., and Fedorova, A., "New methods for estimating flat field and stray light images from the ACS-NIR spectrometer on board TGO," in [*Proceedings of the Conference on 'Smart Sensors and Systems: Technology and Applications (SSS&TA' 2022)*], (2022).

[6] Hestroffer, D. and Magnan, C. N., "Wavelength dependency of the solar limb darkening," *Astronomy and Astrophysics* **333**, 338–342 (1998).

[7] Toon, G. C., "The solar spectrum: An atmospheric remote sensing perspective," (2013).

[8] Gordon, I., Rothman, L., Hill, C., Kochanov, R., Tan, Y., Bernath, P., Birk, M., Boudon, V., Campargue, A., Chance, K., Drouin, B., Flaud, J.-M., Gamache, R., Hodges, J., Jacquemart, D., Perevalov, V., Perrin, A., Shine, K., Smith, M.-A., Tennyson, J., Toon, G., Tran, H., Tyuterev, V., Barbe, A., Császár, A., Devi, V., Furtenbacher, T., Harrison, J., Hartmann, J.-M., Jolly, A., Johnson, T., Karman, T., Kleiner, I., Kyuberis, A., Loos, J., Lyulin, O., Massie, S., Mikhailenko, S., Moazzen-Ahmadi, N., Müller, H., Naumenko, O., Nikitin, A., Polyansky, O., Rey, M., Rotger, M., Sharpe, S., Sung, K., Starikova, E., Tashkun, S., Auwera, J. V., Wagner, G., Wilzewski, J., Wcisło, P., Yu, S., and Zak, E., "The hitran2016 molecular spectroscopic database," *Journal of Quantitative Spectroscopy and Radiative Transfer* **203**, 3–69 (2017). HITRAN2016 Special Issue.